

Article

The Co-B Amorphous Alloy: A High Capacity Anode Material for an Alkaline Rechargeable Battery

Shujun Qiu, Jianling Huang, Hailiang Chu *, Yongjin Zou, Cuili Xiang, Erhu Yan, Fen Xu and Lixian Sun *

Guangxi Key Laboratory of Information Materials, Guangxi Collaborative Innovation Center of Structure and Property for New Energy and Materials, School of Materials Science and Engineering, Guilin University of Electronic Technology, Guilin 541004, China; qiushujun@guet.edu.cn (S.Q.); jianlinghuang@126.com (J.H.); zouy@guet.edu.cn (Y.Z.); xiangcuili@guet.edu.cn (C.X.); yeh@guet.edu.cn (E.Y.); xufen@guet.edu.cn (F.X.)

* Correspondence: chuhailiang@guet.edu.cn (H.C.); sunlx@guet.edu.cn (L.S.);

Tel.: +86-773-2216607 (H.C. & L.S.); Fax: +86-773-2290129 (H.C. & L.S.)

Academic Editor: Hugo F. Lopez

Received: 29 August 2016; Accepted: 3 November 2016; Published: 7 November 2016

Abstract: The Co-B amorphous alloys were prepared via a chemical reduction method by sodium borohydride, using three different cobalt salts ($\text{CoCl}_2 \cdot 6\text{H}_2\text{O}$, $\text{CoSO}_4 \cdot 7\text{H}_2\text{O}$, and $\text{Co}(\text{NO}_3)_2 \cdot 6\text{H}_2\text{O}$) as sources of cobalt. As anode materials in alkaline rechargeable batteries, the Co-B alloy prepared from $\text{CoCl}_2 \cdot 6\text{H}_2\text{O}$ has a maximum specific discharge capacity of 844.6 mAh/g, and 306.4 mAh/g is retained even after 100 cycles at a discharge current of 100 mA/g. When $\text{Co}(\text{NO}_3)_2 \cdot 6\text{H}_2\text{O}$ is used as a raw material, the formation of $\text{Co}_3(\text{BO}_3)_2$ worsens the electrochemical properties of the sample, i.e., a maximum capacity of only 367.0 mAh/g.

Keywords: amorphous materials; energy storage and conversion; rechargeable battery; anode

1. Introduction

Alkaline secondary batteries are regarded as one of the most promising power sources in the application of modern electronic products. In the past few decades, extensive studies on hydrogen storage alloys (HMs) as anode materials of nickel–metal hydride (Ni–MH) batteries have been reported as being used in portable electronics due to their high specific capacity, good durability, and environmental friendliness [1–6]. Up to now, many kinds of metal hydrides have been developed; for instance, Mg-based alloys exhibit a maximum discharge capacity above 500 mAh/g, but the poor cycling ability limits widespread practical application [7]. Comparatively, the AB_5 -type MHs widely used as commercialized anode materials for Ni–MH secondary batteries usually have a reversible discharge capacity of about 310 mAh/g [8].

Recently, a new class of anode materials based on transition metals that possess superior electrochemical properties was developed [9–11]. For instance, ultra-fine particles of the Co–B amorphous alloy were successfully prepared through NaBH_4 reduction of CoSO_4 . As an anode in an alkaline rechargeable battery, the discharge capacity of more than 600 mAh/g is obtained at the initial cycle. In addition, the cycling ability and high rate capability are fairly good [9]. The FeB alloy prepared with an electric arc method achieved an excellent reversible capacity of 312 mAh/g as well as good cyclability [11]. In fact, the electrochemical reaction is based on the multi-electron redox reaction [12]. For instance, Co-based alloys as anodes in alkaline secondary batteries are primarily ascribed to the redox between Co and $\text{Co}(\text{OH})_2$ [13–19]. Wang et al. first reported that the Co-B alloy prepared via a chemical reduction method in an aqueous solution from bivalent cobalt sulfate has a reversible discharge capacity exceeding 300 mAh/g at 100 mA/g in an aqueous KOH solution [9], very close to those of conventional hydrogen storage alloys. Using cobalt acetate as raw

material, Tong et al. prepared a Co-B alloy in water/cetyl-trimethyl-ammonium bromide/n-hexanol microemulsion, which has a maximum discharge capacity of 357 mAh/g and still has 347 mAh/g after 50 cycles [20]. Via the vacuum freeze-drying method from bivalent cobalt chloride, the as-prepared Co-B alloy has a maximum discharge capacity of 438 mAh/g [21]. In a very recent study, an amorphous Co-B alloy prepared by the reduction of CoSO_4 with KBH_4 was found to have an extremely high discharge capacity of 968.6 mAh/g, and the introduction of $\text{Na}_2\text{S}_2\text{O}_3$ into the alkaline electrolyte was found to be helpful for long-term battery storage [22]. Among previous reports, almost all of the Co-B alloys prepared through chemical reduction have an amorphous structure in nature, but there is a huge difference in the electrochemical performance. Moreover, the anions in the cobalt salts have an unclear effect on the particle size, morphology, properties, etc. This has been confirmed by the difference in the Co-B alloys' catalytic activity using different cobalt salts in hydrogen production by hydrolysis of metal borohydrides [23].

In order to understand the effect of anions on the electrochemical performance, the Co-B alloys were prepared via the reduction of cobalt chloride hexahydrate ($\text{CoCl}_2 \cdot 6\text{H}_2\text{O}$), cobalt sulfate heptahydrate ($\text{CoSO}_4 \cdot 7\text{H}_2\text{O}$), and cobalt nitrate hexahydrate ($\text{Co}(\text{NO}_3)_2 \cdot 6\text{H}_2\text{O}$) with sodium borohydride, and the effect of the anions on the electrochemical performance was investigated.

2. Materials and Methods

2.1. Sample Preparation

The experimental procedure for sample preparation is described in the literature [10]. Typically, cobalt salt, i.e., cobalt chloride hexahydrate, cobalt sulfate heptahydrate, and cobalt nitrate hexahydrate, was first introduced into a round-bottom flask, which contains 60 mL of deionized water. Subsequently, 15 mL of freshly prepared 200 g/L NaBH_4 solution was pumped into the aforementioned solution under moderate stirring. Then, the black precipitate was filtrated after no bubble generation, and washed with deionized water and absolute ethanol. Finally, the samples were vacuumed at 60 °C for 8 h to remove water and ethanol. The sample was named as S_C , S_S , and S_N according to the used salt, i.e., chloride, sulfate, and nitrate, respectively.

2.2. Structural and Morphological Characterization

The crystal structure and surface morphology of the samples were characterized by a PANalytical X-ray Diffractometer (XRD, X'Pert MPD PRO, Co $K\alpha$, 45 kV \times 40 mA, Eindhoven, The Netherland) and scanning electron microscopy (SEM, QUANTA FEG450, 10 kV, Eindhoven, The Netherland). The bulk elemental composition of Co and B in the as-prepared sample was measured via inductive coupled plasma atomic emission spectroscopy (ICP–AES, Optima 8000, PerkinElmer, Waltham, MA, USA). The specific surface area (S_{BET}) was measured via nitrogen absorption at 77 K after degassing at 373 K for 4 h (QUANTACHROME AUTOSORB IQ2, Boynton Beach, FL, USA).

2.3. Electrochemical Measurements

The anode was fabricated by pressing a mixture of the Co-B alloy powder and nickel powder in a weight ratio of 1:3 into a circular pellet of $\phi 10$ mm under 25 MPa pressure. Electrochemical measurements were conducted in a tri-electrode cell containing a counter electrode ($\text{Ni}(\text{OH})_2/\text{NiOOH}$) and a reference electrode (Hg/HgO), and a 6 M KOH solution as the electrolyte. The charge–discharge performance was evaluated with a LAND-CT2001A battery system (Wuhan, China). In each cycle test, the anode was charged for 3 h at a constant current density of 300 mA/g, rested for 5 min, and discharged to -0.6 V (versus Hg/HgO) at a constant current density of 100 mA/g.

The cyclic voltammetry (CV) curves, electrochemical impedance spectroscopy (EIS), and linear polarization (LP) curves of the Co-B alloys were recorded on a Zahner IM6e electrochemical workstation (Zahner-Elektrok, Germany). LP was measured by scanning the anode potential at a rate of 0.1 mV/s from -5 to 5 mV (versus open circuit potential). EIS was conducted from 10 kHz to 5 mHz with

an amplitude of 5 mV (versus open circuit potential). The scanning rate of CV curves was 0.5, 1, and 5 mV/s, and the potential range was from -1.2 to -0.4 V (versus Hg/HgO). The EIS and LP curves were measured at a 50% depth of discharge (DOD).

3. Results and Discussion

Analyzed through ICP-AES technique, the chemical composition of the samples was found to be $\text{CoB}_{0.50}$, $\text{CoB}_{0.54}$, and $\text{CoB}_{0.36}$ for S_C , S_S , and S_N , respectively. The following reactions were suggested to form the Co-B alloys [24]:

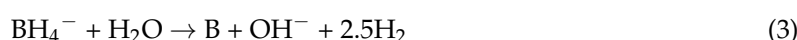
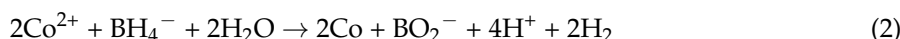


Figure 1A shows XRD patterns of as-prepared Co-B alloys. There is a very broad diffraction peak appearing at $2\theta = 45^\circ\text{--}60^\circ$ with very minor peaks observed at 43° , indicating that the main phase is an amorphous structure in nature as reported in [9,19,22]. As for the sample S_N , it mainly shows an amorphous phase, except for two diffraction peaks at about 40° and 72° , matching the strongest (121) and moderately strong (330) diffraction peaks of the orthorhombic $\text{Co}_3(\text{BO}_3)_2$ observed [25]. SEM images (shown in Figure 1B) show that both S_C and S_S consist of very small primary particles in a few tens of nanometers with good uniform distribution, while S_N shows a much larger aggregated block (secondary particle) on a much larger scale. This highlights that the anions in the precursors have an important influence on the sample morphology and thus give rise to a distinct difference in the electrochemical properties. The specific surface area of the powders was determined by the BET method. The as-prepared S_C and S_S have a surface area of 26.3 and 22.5 m^2/g . Due to the formation of $\text{Co}_3(\text{BO}_3)_2$ for S_N , it has a high value of 169.0 m^2/g , which is similar to the result of $(\text{Ni},\text{Co})_3(\text{BO}_3)_2$ [26]. XPS results of S_S show that the B element is in the oxidized state and the Co element exists in both elemental and oxidized states [27]. This means that the surface of the Co-B sample consists of Co, CoO, and B_2O_3 , which was also reported in [22]. Due to the severe agglomeration, the secondary particle size (D_{50}) of the samples was determined to be 0.8, 1.2, and 3.3 μm for S_C , S_S , and S_N , respectively.

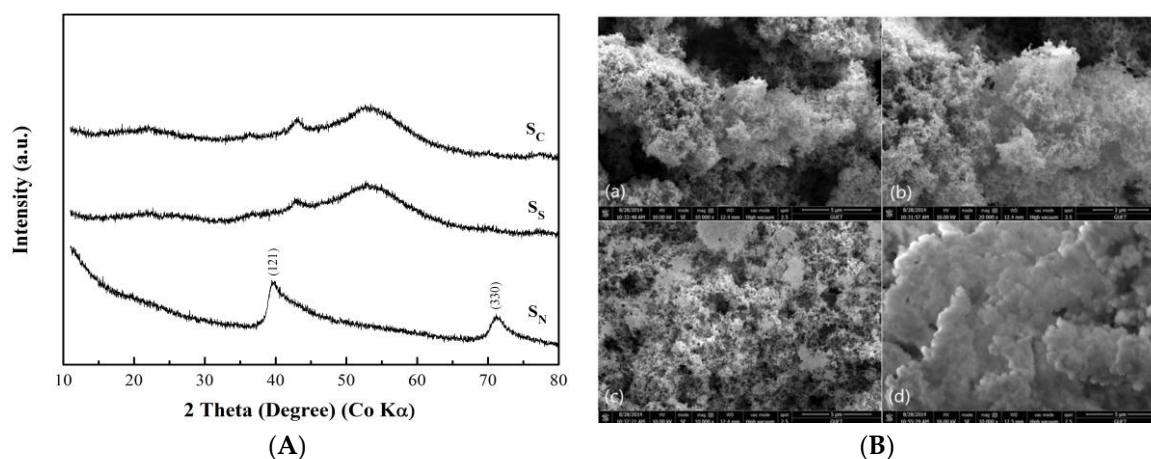


Figure 1. (A) XRD patterns and (B) SEM micrographs of the as-prepared Co-B alloys: (a) and (b) for S_C at different magnifications; (c) for S_S ; and (d) for S_N .

The cycle stability of the Co-B anodes tested at 298 K is shown in Figure 2. Generally, most of anodes made from hydrogen storage alloys need several charge–discharge cycles to reach the maximum of discharge capacity (the so-called activation). In comparison, Co-B alloys show such an excellent electrochemical activity that all of them achieve their maximum discharge capacities at the initial cycle.

The inset gives the maximum discharge capacity of Co-B alloys at 298 K. Obviously, the anions in the different cobalt salts observably affect the microstructure and then the electrochemical properties. For example, S_C has an extremely high maximum discharge capacity of 844.6 mAh/g, which is much higher than that of conventional hydrogen storage alloys [1–6]. The maximum discharge capacity of S_S and S_N are 669.8 and 367.0 mAh/g, respectively. However, the capacity decays rapidly in the first few cycles for S_S and S_C due to the irreversible hydrogen desorption reaction [22]. Subsequently, the reversible capacity is almost retained at a constant in 40 charge–discharge cycles. It is worth noting that S_C is retained at about 440 mAh/g, even after 40 cycles. The discharge capacity of S_C and S_N is 306.4 mAh/g and 187.6 mAh/g at the 100th charge–discharge cycle, respectively, and it is 287.2 mAh/g for S_S at the 92th cycle. As a comparison, the discharge capacity of MnO_2 as the cathode in the KOH electrolyte is only 330 and 60 mAh/g for the 1st and 2nd cycles. The redox mechanism studied using transmission electron microscopy (TEM, JEOL 2010F, Tokyo, Japan) and its associated techniques involves a K^+ ion insertion–surface film formation on the host framework structure of MnO_2 [28], and this process is not fully reversible, responsible for the sharp decrease of the discharge capacity. This mechanism is very different from that in our case, discussed in the following parts.

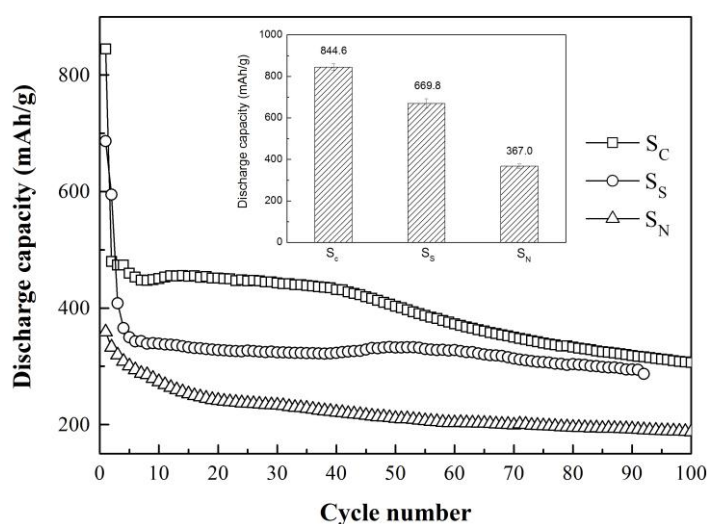


Figure 2. Cycling life of Co-B alloys as the anodes. The inset shows the maximum discharge capacity.

Figure 3 shows the charge–discharge curves of the Co-B alloy anodes at the 15th and 35th cycles. All charge curves have two plateaus in the potential range of 0.88–1.1 V (versus Hg/HgO), while one flat discharge plateau is observed for each Co-B anode. S_C has a much higher discharge plateau appearing at ~ 0.8 V (versus Hg/HgO). Moreover, it has almost the same discharge plateau between the 15th and 35th cycles, which indicates that an excellent reversible electrochemical reaction of S_C . In the case of S_S and S_N , the increase of hysteresis between charge and discharge voltage plateaus indicates a severe polarization of the alloy electrode, which probably results in the deterioration of electrochemical properties.

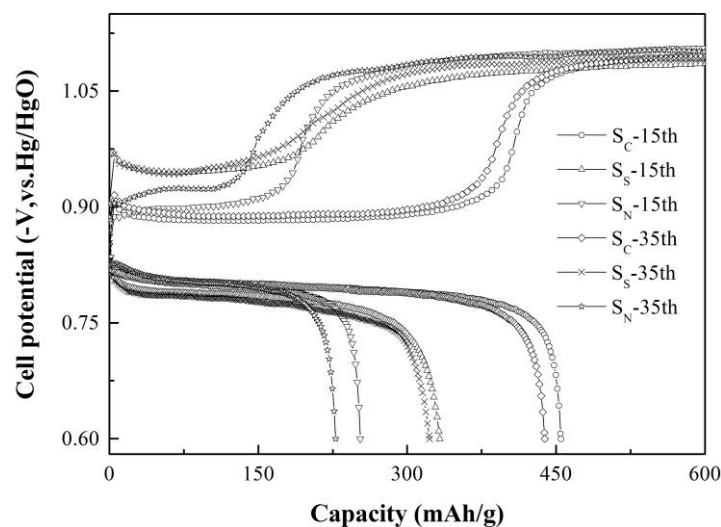


Figure 3. Potential-capacity curves of Co-B alloy anodes at the 15th and 35th cycles.

According to the above experimental results, it can be concluded that the electrochemical performance is in following order: $S_C > S_S > S_N$. As is well-known, Cl is the most electronegative element among the three anions, so Co^{2+} is more electrophilic in CoCl_2 and attracts BH_4^- , which results in an improved electrochemical performance [29]. During the synthesis of Co-B alloys, it was confirmed that the anion plays a crucial role in altering the reaction pathways for the formation of Co-B or $\text{Co}(\text{OH})_2$ [30]. Generally, once a cobalt salt solution is mixed with a NaBH_4 solution, $\text{Co}(\text{OH})_2$ is first formed and then transforms into Co-B alloys. However, in the case of $\text{Co}(\text{NO}_3)_2 \cdot 6\text{H}_2\text{O}$ as the cobalt source, $\text{Co}_3(\text{BO}_3)_2$ as a by-product was obtained during the formation of the Co-B alloy. Moreover, NO_3^- has a negative effect on the formation of the Co-B alloy and thus results in the aggregation of $\text{Co}(\text{OH})_2$ powder, which therefore leads to the morphology with many aggregated particles as shown in Figure 1B. However, the formation of $\text{Co}(\text{OH})_2$ layer hampers the charge transfer at the particle surface and thus may decline the electrochemical activity of the Co-B alloy. In addition, the electrochemical performance of Co-B alloys as anodes is also dependent on their particle size. The smaller the particle size, the higher the electrochemical activity [20]. Compared with S_N , the particle size of S_C is much smaller (Figure 1B), which may be partially responsible for the improvement of electrochemical properties. Thus, S_C has the highest reversible discharge capacity, and S_N has the lowest capacity in this work. The difference between S_N and S_S may be due to the difference in particle size, surface area, or both.

The electrochemical reaction mechanism was investigated via cyclic voltammetry (CV), electrochemical impedance spectroscopy (EIS), and linear polarization (LP), shown in Figure 4. In the CV curves, a remarkable oxidation peak appears at -0.73 V (versus Hg/HgO) and a strong reduction peak appears at -0.99 V (versus Hg/HgO) at a scanning rate of 0.5 mV/s. This pair of redox peaks suggests a reversible electrochemical reaction occurring on the S_C anode. The charge-transfer reaction resistance R_{ct} on the anode surface determined from the EIS data by an equivalent circuit proposed by Kuriyama et al. [31] shows that, among the studied Co-B alloys, a low value of 201.4 m Ω is obtained for S_C , while a high value of 264.1 m Ω for S_N is probably due to the formation of the $\text{Co}(\text{OH})_2$ layer. Moreover, the exchange current density I_0 of S_C , S_S , and S_N obtained from linear polarization is 122.6 , 32.6 , and 18.9 mA/g, respectively, which agrees well with EIS results. Through the CV, EIS, and LP measurements, it can be safely inferred that S_C has much better electrochemical kinetics among the three samples.

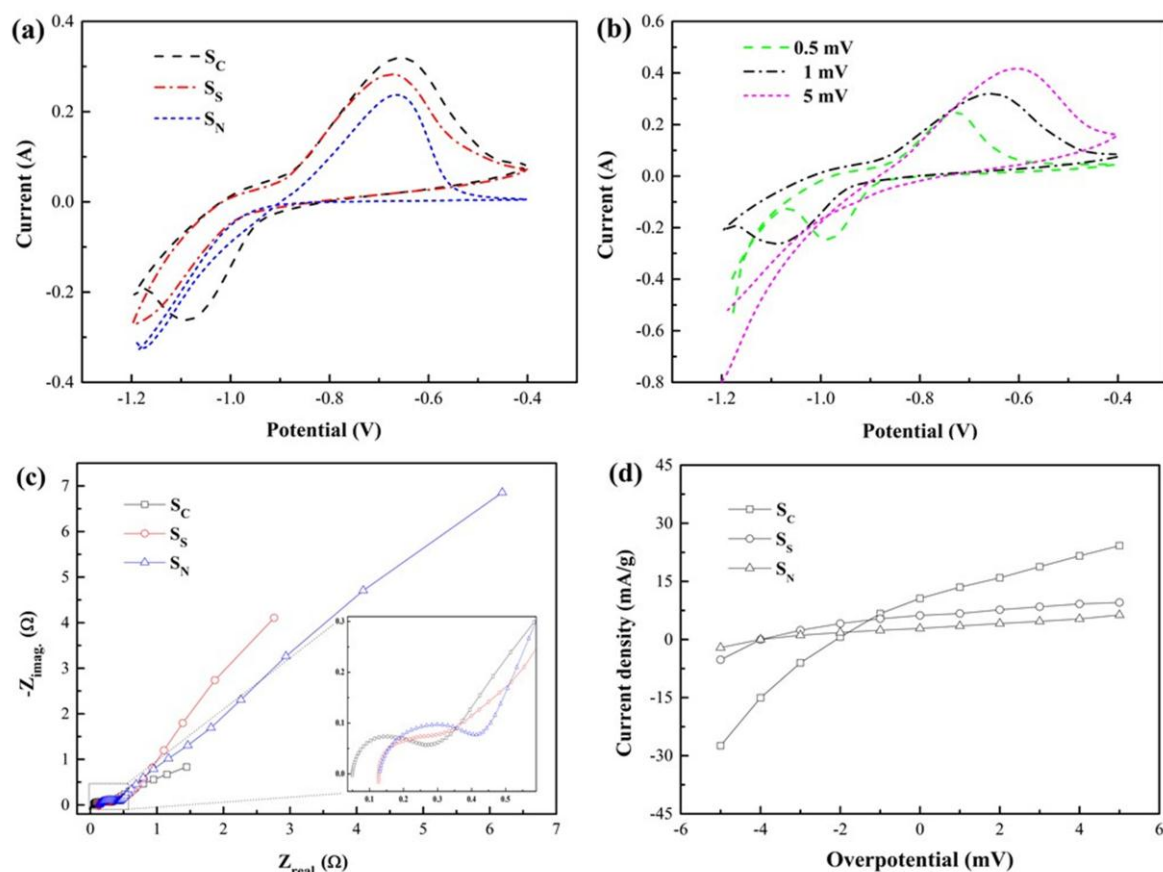


Figure 4. Typical CV curves of Co-B alloys: (a) the scanning rate was 1 mV/s; (b) the CV curves of the S_C at different scanning rates; (c) EIS and (d) LP of Co-B alloy electrodes at 50% DOD and 298 K.

4. Conclusions

Co-B alloys with high discharge capacity were successfully prepared via a chemical reduction method from cobalt chloride hexahydrate, cobalt sulfate heptahydrate, and cobalt nitrate hexahydrate. The structural features, the electrochemical performance, and the electrochemical reaction mechanism were systematically investigated. XRD and SEM show that Co-B alloys are at the nanoscale with uniform nanoparticles. All the anodes achieve maximum discharge capacities at the initial cycle, and the maximum discharge capacity of S_C, S_S, and S_N was 844.6, 669.8, and 367.0 mAh/g, respectively. The discharge capacity of S_C is retained at 431.8 mAh/g, even after 40 charge/discharge cycles. The experimental results obtained in this work indicate that the Co-B alloy prepared from cobalt chloride hexahydrate is one of the most promising candidates for practical applications in alkaline secondary batteries.

Acknowledgments: This research was financially supported by the National Natural Science Foundation of China (51361006, 51401059, 51461010, 51361005, 51371060, U1501242, and 51461011) and the Guangxi Natural Science Foundation (2014GXNSFAA118043, 2015GXNSFBA139208 and 2014GXNSFAA118333).

Author Contributions: H.C., F.X., and L.S. conceived and designed the experiments; S.Q., J.H., and C.X. performed the experiments; S.Q., Y.Z., and H.C. analyzed the data; S.Q., J.H., and E.Y. contributed reagents/materials/analysis tools; S.Q. and H.C. wrote the paper.

Conflicts of Interest: The authors declare no conflict of interest.

References

1. Tliha, M.; Khaldi, C.; Boussami, S.; Fenineche, N.; El-Kedim, O.; Mathlouthi, H.; Lamloumi, J. Kinetic and thermodynamic studies of hydrogen storage alloys as negative electrode materials for Ni/MH batteries: A review. *J. Solid State Electrochem.* **2014**, *18*, 577–593. [[CrossRef](#)]
2. Huang, J.L.; Qiu, S.J.; Chu, H.L.; Zou, Y.J.; Xiang, C.L.; Zhang, H.Z.; Xu, F.; Sun, L.X.; Ouyang, L.Z.; Zhou, H.Y. Enhancement of the electrochemical properties of rare earth-based alloy by doping with CoZnB alloy. *Int. J. Hydrog. Energy* **2015**, *40*, 14173–14178. [[CrossRef](#)]
3. Liu, Y.F.; Pan, H.G.; Gao, M.X.; Wang, Q.D. Advanced hydrogen storage alloys for Ni/MH rechargeable batteries. *J. Mater. Chem.* **2011**, *21*, 4743–4755. [[CrossRef](#)]
4. Qiu, S.J.; Huang, J.L.; Chu, H.L.; Zou, Y.J.; Xiang, C.L.; Zhang, H.Z.; Xu, F.; Sun, L.X.; Zhou, H.Y. Influence of boron introduction on structure and electrochemical hydrogen storage properties of Ti–V-based alloys. *J. Alloy. Compd.* **2015**, *648*, 320–325. [[CrossRef](#)]
5. Zhao, X.Y.; Li, J.J.; Yao, Y.; Ma, L.Q.; Shen, X.D. Electrochemical hydrogen storage properties of a non-equilibrium Ti₂Ni alloy. *RSC Adv.* **2012**, *2*, 2149–2153. [[CrossRef](#)]
6. Qiu, S.J.; Huang, J.L.; Chu, H.L.; Zou, Y.J.; Xiang, C.L.; Zhang, H.Z.; Xu, F.; Sun, L.X.; Ouyang, L.Z.; Zhou, H.Y. Influence of Zr addition on structure and performance of rare earth Mg-based alloys as anodes in Ni/MH battery. *Metals* **2015**, *5*, 565–577. [[CrossRef](#)]
7. Zhuang, X.Y.; Zhang, Y.; Zhu, Y.F.; Qu, Y.; Zhan, L.Y.; Wan, N.; Cheng, H.H.; Guo, X.L.; Chen, J.; Wang, Z.M.; et al. The effects of Pd and/or Zr additives on the structures and cyclic stabilities of Mg₅₀Ni₅₀-based electrode alloys. *Int. J. Hydrog. Energy* **2015**, *40*, 2768–2774. [[CrossRef](#)]
8. Dymek, M.; Bala, H.; Hackemer, A.; Drulis, H. Hydrogenation and electrochemical corrosion properties of LaNi_{4.5}Co_{0.5} alloy doped with aluminum. *Solid State Ionics* **2015**, *271*, 116–120. [[CrossRef](#)]
9. Wang, Y.D.; Ai, X.P.; Yang, H.X. Electrochemical hydrogen storage behaviors of ultrafine amorphous Co–B alloy particles. *Chem. Mater.* **2004**, *16*, 5194–5197. [[CrossRef](#)]
10. Qiu, S.J.; Huang, J.L.; Shen, F.H.; Pang, R.; Chu, H.L.; Zou, Y.J.; Xiang, C.L.; Xu, F.; Du, Y.; Wang, J.C.; et al. Ternary Co–Ni–B amorphous alloy with a superior electrochemical performance in a wide temperature range. *Int. J. Hydrog. Energy* **2016**, *41*, 3955–3960. [[CrossRef](#)]
11. Qiu, S.J.; Huang, J.L.; Shen, F.H.; Pang, R.; Chu, H.L.; Zou, Y.J.; Xiang, C.L.; Yan, E.H.; Xu, F.; Sun, L.X.; et al. Enhancement of the electrochemical performance of CoB amorphous alloy through the addition of A₂B₇-type alloy. *Int. J. Hydrog. Energy* **2016**, *41*, 16142–16147.
12. Gao, X.P.; Yang, H.X. Multi-electron reaction materials for high energy density batteries. *Energy Environ. Sci.* **2010**, *3*, 174–189.
13. Zhao, X.Y.; Ma, L.Q.; Yao, Y.; Yang, M.; Ding, Y.; Shen, X.D. Electrochemical energy storage of Co powders in alkaline electrolyte. *Electrochim. Acta* **2010**, *55*, 1169–1174. [[CrossRef](#)]
14. He, G.H.; Jiao, L.F.; Yuan, H.T.; Zhang, Y.Y.; Zhang, Y.H.; Wang, Y.J. Effect of synthesis method on the structure and electrochemical behaviour of Co–Si particles. *Int. J. Hydrog. Energy* **2007**, *32*, 3416–3419. [[CrossRef](#)]
15. Lu, D.S.; Li, W.S.; Xiao, F.M.; Tang, R.H. Drastically enhanced cycle life of Co–B alloy electrode by 8-hydroxyquinoline at elevated temperature. *Electrochem. Commun.* **2010**, *12*, 362–366. [[CrossRef](#)]
16. Wang, Q.H.; Jiao, L.F.; Du, H.M.; Huan, Q.N.; Peng, W.X.; Song, D.W.; Wang, Y.J.; Yuan, H.T. Chainlike structures assembled by Co architectures: Synthesis and electrochemical properties as negative materials for alkaline secondary batteries. *J. Mater. Chem.* **2011**, *21*, 14159–14162. [[CrossRef](#)]
17. Wang, Q.H.; Jiao, L.F.; Du, H.M.; Huan, Q.N.; Peng, W.X.; Song, D.W.; Wang, Y.J.; Yuan, H.T. Novel flower-like CoS architectures: One-pot synthesis and electrochemical properties. *J. Mater. Chem.* **2011**, *21*, 327–329. [[CrossRef](#)]
18. Cao, Y.L.; Zhou, W.C.; Li, X.Y.; Ai, X.P.; Gao, Y.P.; Yang, H.X. Electrochemical hydrogen storage behaviors of ultrafine Co–P particles prepared by direct ball-milling method. *Electrochim. Acta* **2006**, *51*, 4285–4290. [[CrossRef](#)]
19. Lu, D.S.; Li, W.S.; Tan, C.L.; Zeng, R.H. Investigation of Co–B–S system as anode material for secondary alkaline battery. *Electrochim. Acta* **2009**, *55*, 171–177. [[CrossRef](#)]

20. Tong, D.G.; Wang, D.; Chu, W.; Sun, J.H.; Wu, P. Cobalt–boron amorphous alloy prepared in water/cetyl-trimethyl-ammonium bromide/*n*-hexanol microemulsion as anode for alkaline secondary batteries. *Electrochim. Acta* **2010**, *55*, 2299–2305. [[CrossRef](#)]
21. Wu, C.; Pang, C.H.; Wu, F.; Bai, Y.; Chen, C.; Zhong, Y. Effects of the pre-freezing time on the structures and electrochemical performances of Co-B alloys. *Adv. Mater. Res.* **2012**, *391*, 1085–1089. [[CrossRef](#)]
22. Zhao, X.Y.; Li, J.J.; Yao, Y.; Ma, L.Q.; Shen, X.D. Electrochemical redox mechanism of Co-B-H anode material and its optimization by a novel electrolyte additive. *RSC Adv.* **2013**, *3*, 1327–1331. [[CrossRef](#)]
23. Patel, N.; Miotello, A. Progress in Co-B related catalyst for hydrogen production by hydrolysis of boron-hydrides: A review and the perspectives to substitute noble metals. *Int. J. Hydrog. Energy* **2015**, *40*, 1429–1464. [[CrossRef](#)]
24. Chen, Y. Chemical preparation and characterization of metal–metalloid ultrafine amorphous alloy particles. *Catal. Today* **1998**, *44*, 3–16. [[CrossRef](#)]
25. Zhang, X.X.; Gu, G.; Huang, H.J.; Yang, S.H.; Du, Y.W. Self-assembled $\text{Co}_3(\text{BO}_3)_2$ /surfactant nanostructured multilayers. *J. Phys. Condens. Matter* **2001**, *13*, 3913. [[CrossRef](#)]
26. Chen, Y.Z.; Liu, Y.N.; Yan, W. Preparation of porous $(\text{Ni},\text{Co})_3(\text{BO}_3)_2/\text{Ni}(\text{OH})_2$ nanosheet networks as pseudocapacitor materials with superior performance. *J. Mater. Chem. A* **2014**, *2*, 5903–5909. [[CrossRef](#)]
27. Zou, Y.J.; Cheng, J.; Wang, Q.Y.; Xiang, C.L.; Chu, H.L.; Qiu, S.J.; Zhang, H.Z.; Xu, F.; Liu, S.S.; Tang, C.Y.; et al. Cobalt–boron/nickel–boron nanocomposite with improved catalytic performance for the hydrolysis of ammonia borane. *Int. J. Hydrog. Energy* **2015**, *40*, 13423–13430. [[CrossRef](#)]
28. Minakshi, M. Examining manganese dioxide electrode in KOH electrolyte using TEM technique. *J. Electroanal. Chem.* **2008**, *616*, 99–106. [[CrossRef](#)]
29. Akdim, O.; Demirci, U.B.; Muller, D.; Miele, P. Cobalt (II) salts, performing materials for generating hydrogen from sodium borohydride. *Int. J. Hydrog. Energy* **2009**, *34*, 2631–2637. [[CrossRef](#)]
30. Wu, C.; Bai, Y.; Wu, F.; Yi, B.L.; Zhang, H.M. Highly active cobalt-based catalysts in situ prepared from CoX_2 ($X = \text{Cl}^-$, NO_3^-) and used for promoting hydrogen generation from NaBH_4 solution. *Int. J. Hydrog. Energy* **2010**, *35*, 2675–2679. [[CrossRef](#)]
31. Kuriyama, N.; Sakai, T.; Miyamura, H.; Uehara, I.; Ishikawa, H.; Iwasaki, T. Electrochemical impedance and deterioration behavior of metal hydride electrodes. *J. Alloy. Compd.* **1993**, *202*, 183–197. [[CrossRef](#)]



© 2016 by the authors; licensee MDPI, Basel, Switzerland. This article is an open access article distributed under the terms and conditions of the Creative Commons Attribution (CC-BY) license (<http://creativecommons.org/licenses/by/4.0/>).